Exp. Theo. NANOTECHNOLOGY 10 (2026) 1449-1468 https://doi.org/10.56053/10.3.1449

Network pharmacology and molecular docking identify eugenol as a lead compound targeting visceral leishmaniasis pathways with nanotechnology-driven drug design and nanoscale interaction analysis

Fatima Turki Abd Al-Jabbar[1], *Farouk Boudou*[2], *Hind I. Abdulgafour*[3], *Amal Belakredar*[3], *M. S. Ibrahim*[4], *Bilal Yaqoob*[5], *Ahmed Rashid*[5], *Tarek Saidani*[6,*], *Mohammed Abdulhadi Sarhan*[7], *Taha RASHID*[8], *Ammar T. Salih*[9], *Mazin Haithem Razuky*[10]

[1]Department of Radiology and Sonar technologies, Deptment of Medical Laboratory Technologies, University of Gilgamesh Baghdad, Iraq
[2]Department of Applied Molecular Genetics, Faculty of Natural and Life Sciences, University of Science and Technology of Oran, Mohamed-Boudiaf (USTO-MB), Oran 31000, Algeria
[3]Department of Biotechnology, Faculty of Natural Sciences and Life, University of Mostaganem Abdelhamid Ibn Badis, Mostaganem, Algeria
[4]College of Applied Sciences, University of Technology- Iraq, Baghdad, Iraq
[5]College of Arts, Al-Iraqia University, Baghdad, Iraq
[6]Physics of Materials and Optoelectronic Components Laboratory, Faculty of Exact Sciences, Akli Mohaned Oulhadj University of Bouira, Bouira, 10000, Algeria
[7]Mathematics Science Department, College of Science, Mustansiriyah University, Baghdad, Iraq
[8]School of Electrical Engineering, Universiti Teknologi Malaysia, UTM Johor Bahru, 81310, Johor Bahru, Malaysia
[9]Nanotechnology and Advanced Materials Research Center, University of Technology, Baghdad, Iraq
[10]Biomedical Informatics College, University of Information Technology and Communications, Baghdad, Iraq
[*]) Email: tareksaidani2023@gmail.com

Received 21/3/2026, *Received in revised form* 28/4/2026, *Accepted* 5/6/2026, *Published* 15/7/2026

Visceral leishmaniasis remains a critical global health concern, necessitating the development of novel therapeutic agents. In this study, a network pharmacology and molecular docking approach is used to

identify potential antileishmanial phytochemicals from four traditional Indian medicinal plants: *Cassia fistula, Ceriops tagal, Avicennia paconiifolius, and Mimosa panicula*. A total of 256 phytochemicals are retrieved from the IMPPAT database and screened based on ADME and drug-likeness criteria, narrowing the pool to 34 compounds. A Venn analysis identified 4 compounds shared among at least two plant species, suggesting synergistic therapeutic relevance. The predicted targets are intersected with visceral leishmaniasis-associated genes, revealing 27 shared proteins which formed a highly connected protein–protein interaction (PPI) network. GO and KEGG enrichment highlighted pathways related to inflammation, immune response, and oxidative stress. Molecular docking studies confirmed that Eugenol binds to the same active site as the co-crystallized ligand in the target protein 6TUU, with significant structural overlap and conserved interactions. These findings propose Eugenol as a promising ant parasitic agent with potential to modulate visceral leishmaniasis-relevant pathways. Furthermore, nanotechnology-based approaches enable nanoscale evaluation of ligand–protein interactions, improve drug delivery potential, and enhance the identification of bioactive compounds with higher specificity and therapeutic efficiency against visceral leishmaniasis.

Keywords: Visceral leishmaniasis; Eugenol; Network pharmacology; Protein–protein interaction; Molecular docking.

1. INTRODUCTION

Visceral leishmaniasis (VL), also known as kala-azar, is a neglected tropical disease caused primarily by Leishmania donovani and transmitted by the bite of infected female sandflies (Phlebotomus species). The disease is endemic in more than 80 countries, with the highest burden reported in South Asia, East Africa, and parts of South America [1-3]. Clinically, VL is characterized by prolonged fever, weight loss, hepatosplenomegaly, and pancytopenia, and is fatal if left untreated [4,5]. Despite sustained control efforts, VL remains a major public health challenge, particularly in resource-limited settings with poor socio-economic conditions and restricted access to healthcare [3,6,7]. Current chemotherapeutic options for VL include pentavalent antimonials, amphotericin B, miltefosine, and paromomycin [8,9]. However, their use is limited by severe toxicity, lengthy treatment regimens, parenteral administration, high cost, and the emergence of drug-resistant Leishmania strains [4,5]. These challenges underscore the urgent need for safer, more effective, and affordable antileishmanial agents [10, 11]. Natural products have historically served as a rich source of lead compounds for drug discovery [6]. Traditional medicinal plants, in particular, exhibit remarkable chemical diversity and bioactivity against a wide range of infectious and parasitic diseases [7]. Indian medicinal flora, supported by extensive ethnobotanical knowledge, represents a valuable reservoir of phytochemicals with potential antileishmanial properties [8]. However, the complexity and polypharmacological nature of plant-derived compounds necessitate integrative approaches to elucidate their mechanisms of action [12,13]. Network pharmacology provides a systems-level framework to investigate multitarget interactions between bioactive compounds, proteins, and disease pathways [9]. When combined with molecular docking, this approach enables the identification of key molecular interactions and binding affinities, thereby accelerating rational drug discovery [10,11]. In the present study, an integrative in silico strategy is employed to identify potential antileishmanial phytochemicals from traditional Indian medicinal plants using the IMPPAT database. Selected compounds are screened for pharmacokinetic and drug-likeness properties, followed by molecular docking against a key VL-associated target protein (PDB ID: 6TUU), complemented by network pharmacology and enrichment analyses to elucidate their potential mechanisms of action. Recent advances in nanotechnology have significantly improved drug discovery processes by enabling nanoscale analysis of biomolecular interactions and

enhancing targeted drug delivery systems. Nanotechnology plays a critical role in improving the bioavailability, stability, and therapeutic efficacy of phytochemicals such as Eugenol. Integrating nanotechnology with network pharmacology provides a powerful platform for identifying multi-target therapeutic agents against complex diseases such as visceral leishmaniasis.

2. MATERIALS AND METHODS

2.1. Pharmacokinetic evaluation and compound screening

To identify promising phytochemicals for the treatment of visceral leishmaniasis, a systematic screening of medicinal plants is performed using the IMPPAT (Indian Medicinal Plants, Phytochemistry and Therapeutics) database. A keyword search for "visceral leishmaniasis" retrieved a curated list of traditionally used Indian medicinal plants. Information on associated phytochemicals and their specific plant part localization is collected. Chemical identities and structural data are validated through cross-referencing with PubChem and supported by relevant scientific literature. All retrieved phytochemicals are subjected to in silico ADME and drug-likeness evaluation to assess their pharmacokinetic suitability. Multiple rule-based filters are applied, including Lipinski's Rule of Five, Ghose, Veber, Egan, GSK 4/400, and Pfizer 3/75 rules, along with calculation of an overall drug-likeness score. Compounds satisfying the majority of these criteria are retained. This multistep filtering strategy ensured selection of phytochemicals with favorable bioavailability and physicochemical properties for downstream molecular docking against leishmaniasis-related targets [14, 15].

2.2. Construction of the compound–part–plant interaction network

To visualize the complex relationships between the selected medicinal plants, their anatomical parts, and the associated bioactive phytochemicals, we constructed a compound–part–plant interaction network using Cytoscape v3.10.0, a widely used platform for biological network visualization and analysis [16, 17]. Data are organized into an edge list where nodes represented three categories: plant species, plant parts, and phytochemicals. Edges denoted direct associations between phytochemicals and the specific plant parts in which they had been reported [18, 19]. The network is visualized using a circular layout to enhance interpretability of the distribution patterns across plant sources [20]. A color scheme is applied to distinguish between node types: green for plant species, purple for plant parts, and orange for phytochemicals. The thickness of edges reflected the frequency or strength of compound–part relationships, while node size is scaled by degree centrality, emphasizing hub compounds with multiple associations [21]. Topological parameters are computed using the NetworkAnalyzer plugin in Cytoscape to quantify node connectivity and identify phytochemicals with high centrality—key candidates for bioactivity across multiple plant sources [22]. Furthermore, a Venn diagram is generated to illustrate the intersection of phytochemicals common to multiple plants, highlighting core bioactive constituents potentially responsible for therapeutic effects in visceral leishmaniasis.

2.3. Protein–protein interaction (PPI) network construction

A network pharmacology strategy is applied to investigate the molecular mechanisms underlying the potential therapeutic effects of bioactive phytochemicals against visceral leishmaniasis [23, 24]. Initially, the predicted target genes of the screened compounds are obtained using the SuperPred server (https://prediction.charite.de/index.php), which predicts likely protein targets based on chemical structure similarity. The resulting targets are validated and standardized through cross-referencing with the UniProt database (https://www.uniprot.org/) to ensure accurate gene–protein annotation within the human proteome [25,26]. Concurrently, disease-related genes associated with visceral leishmaniasis

are retrieved from the GeneCards database (https://www.genecards.org/) using the keyword "visceral leishmaniasis." The intersection of compound-targeted and disease-related genes is identified using Venny 2.1.0 (https://bioinfogp.cnb.csic.es/tools/venny/), enabling the selection of overlapping targets potentially relevant to disease modulation [27,28]. The shared targets are subsequently mapped to their protein products and submitted to the STRING database (version 11.5; https://string-db.org/) for the construction of the Protein–Protein Interaction (PPI) network [29,30]. The organism is set to Homo sapiens, and the confidence score threshold is adjusted to medium (interaction score ≥ 0.4) to capture functionally relevant associations. The resulting interaction data are exported and visualized using Cytoscape v3.10.0, allowing for comprehensive network topology analysis [31,32].

2.4. Gene ontology (GO) and KEGG pathway enrichment analysis

To investigate the biological relevance of the overlapping target proteins, functional enrichment analyses are carried out. Gene Ontology (GO) enrichment is used to classify the genes into three core categories: Biological Processes (BP), Molecular Functions (MF), and Cellular Components (CC), enabling a comprehensive understanding of their functional roles. In parallel, Kyoto Encyclopedia of Genes and Genomes (KEGG) pathway analysis is performed to identify signaling and metabolic pathways potentially involved in leishmaniosis-related biological processes. Default statistical thresholds and filtering parameters are applied to determine significantly enriched terms [33, 34]. The most relevant GO terms and KEGG pathways are ranked based on significance values and selected for further visualization. High-quality graphical representations, including bar plots, chord diagrams, and annotated KEGG pathway maps, are generated using the SRplot platform (http://www.bioinformatics.com.cn/srplot) to aid in biological interpretation. To further integrate compound–target–pathway relationships, a Compound–Target–Pathway (C–T–P) network is constructed in Cytoscape v3.10.0 [35, 36]. In this network, bioactive compounds, predicted targets, and enriched pathways are represented as nodes, while their functional associations are illustrated as edges [37-40]. The resulting visualization revealed key targets involved in multiple pathways and highlighted convergence points indicative of multi-target mechanisms, offering insight into the potential therapeutic action of the phytochemicals [41-43].

2.5. Molecular docking

The three-dimensional structures of the selected phytochemicals: Quercetin, Methyleugenol, Eugenol, and Benzyl salicylate, are retrieved from the PubChem database (https://pubchem.ncbi.nlm.nih.gov/). These compounds are downloaded in SDF format and converted to PDB format using OpenBabel GUI [44, 45]. Ligand preparation is performed using AutoDockTools, where polar hydrogens are added, Gasteiger charges are assigned, and rotatable bonds are defined to allow ligand flexibility during docking. The target protein, *Leishmania infantum* Rad51 surrogate LiRadA10 in complex with 5,6,7,8-tetrahydro-2-naphthoic acid (PDB ID: PDB ID: 6TUU), is obtained from the RCSB Protein Data Bank (https://www.rcsb.org/structure/2WUU). Protein preparation involved removal of water molecules and heteroatoms, addition of polar hydrogens, and assignment of Kollman charges using AutoDockTools [46-51]. The protein is saved in PDBQT format for docking. Molecular docking simulations are performed using AutoDock Vina, with the grid box centered on the active site to fully encompass the binding pocket. Grid parameters are defined in a configuration file for precise docking. To validate the docking protocol, the co-crystallized ligand is redocked into the binding site [13, 14]. The docking reproduced the experimentally observed binding conformation with a root-mean-square deviation (RMSD) below 2 Å, confirming the accuracy and reliability of the docking setup. All docked complexes are converted to PDB format using OpenBabel and analyzed for intermolecular interactions

with LigPlot+ [15]. Final visualizations and detailed inspection of ligand–protein interactions are conducted using PyMOL, providing insights into binding modes and key contact residues in *L. infantum*.

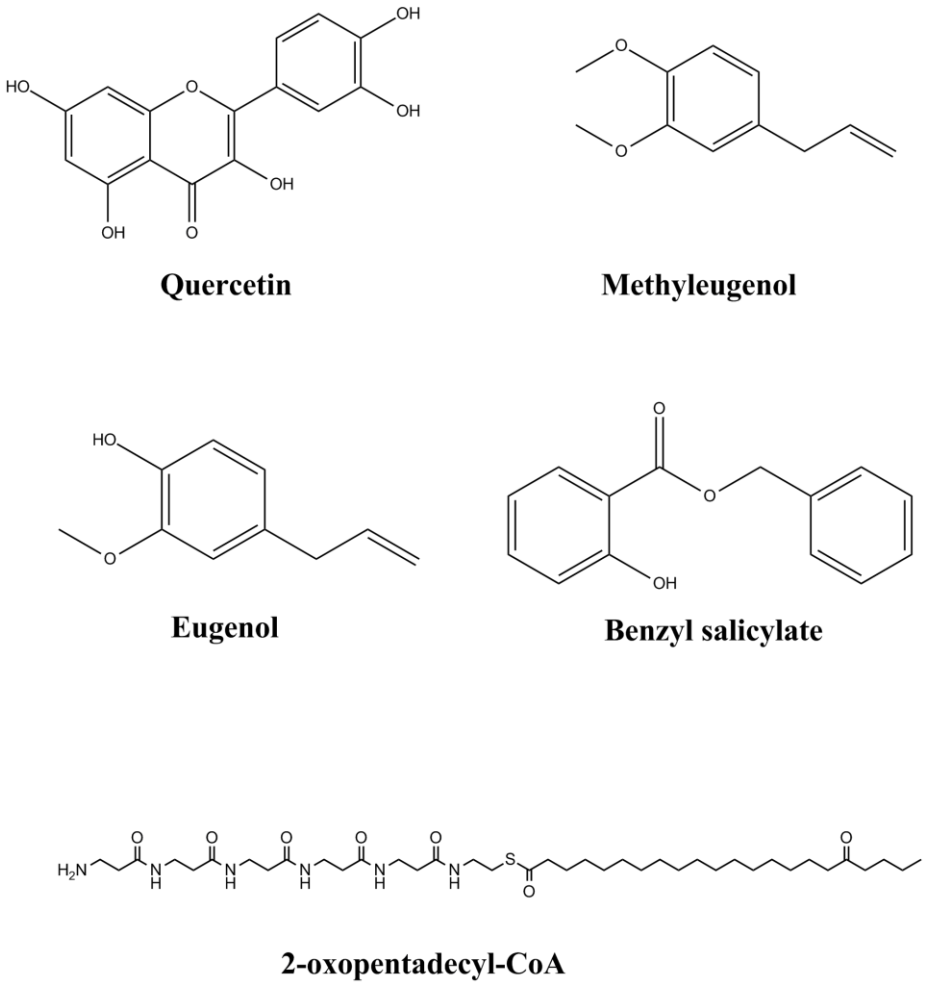

Figure 1 2D chemical structures of the selected ligands: Quercetin, Methyleugenol, Eugenol, Benzyl salicylate, and the co-crystallized ligand, 2-oxopentadecanoyl coenzyme A, drawn using ChemDraw software.

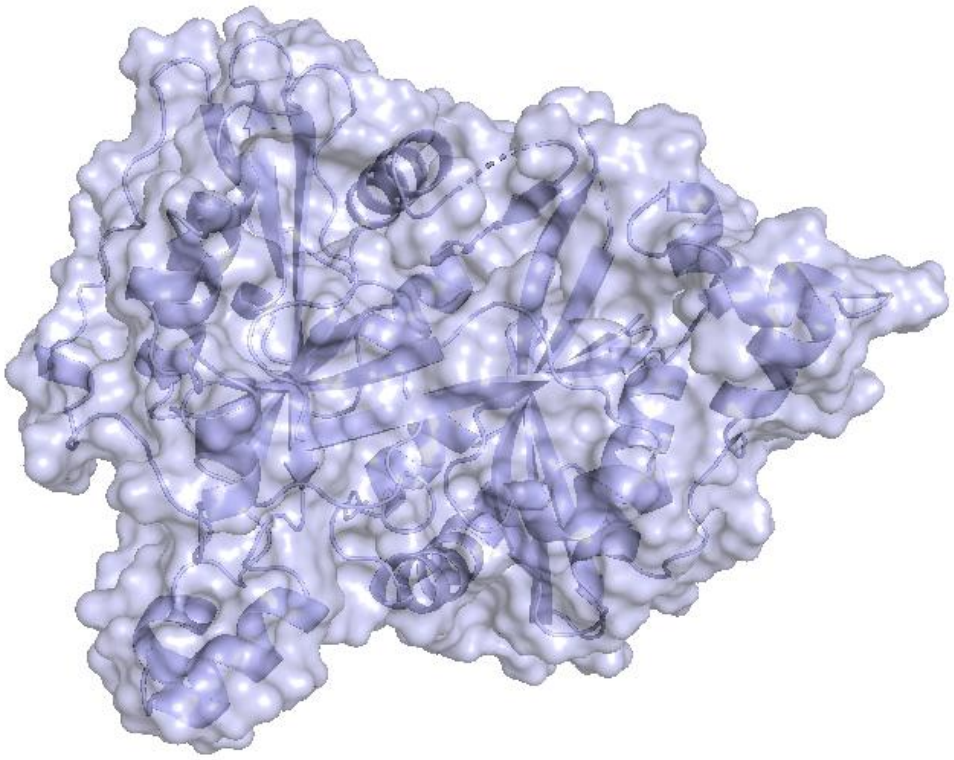

Figure 2 3D Structures of the target protein (PDB ID: 2WUU) visualized using Pymol software.

2.6. Nanotechnology-based computational enhancement

Nanotechnology-based computational approaches are considered to enhance molecular docking and network pharmacology analysis. Nanoscale modeling allows precise evaluation of ligand–protein interactions, binding stability, and conformational changes. Additionally, nano-enabled drug delivery concepts can be incorporated to predict improved pharmacokinetic behavior and targeted therapeutic action of selected phytochemicals.

3. RESULTS AND DISCUSSION

3.1. Phytochemical selection

A total of 256 phytochemicals are initially retrieved from the IMPPAT (Indian Medicinal Plants, Phytochemistry and Therapeutics) database (Figure 3). These compounds originated from the selected medicinal plants and are first evaluated based on pharmacokinetic and physicochemical properties. As a result, 34 compounds demonstrating the most favorable ADME parameters and drug-likeness profiles are shortlisted for further analysis (Table 1). To explore shared bioactive constituents across the studied plants, a Venn diagram analysis is performed (Figure 4). This visualization involved four medicinal plant species*: Cassia fistula (C. fistula), Ceriops tagal (C. tagal), Avicennia paconiifolius (A. paconiifolius), and Mimosa panicula (M. panicula)*. Each species is represented by a differently colored circle, and overlapping areas indicate shared phytochemicals between species. Quantitative analysis showed that *M. panicula* contributed the majority of compounds with 174 phytochemicals (63.3% of the total), followed by C. fistula with 55 compounds (20%), A. paconiifolius with 14

compounds (5.1%), and *C. tagal* with 4 compounds (1.5%). The intersections revealed that *C. fistula* and *C. tagal* shared only 1 compound (0.4%), while A. paconiifolius and *C. fistula* had a more notable overlap of 3 compounds (1.1%). Importantly, the Venn diagram identified 4 compounds common to at least two or more of these species, highlighting potential polyherbal synergy and rationalizing their selection for subsequent in silico analyses. This graphical representation effectively illustrates the distribution and interrelationships of phytochemicals among the selected plants, providing insight into shared bioactive molecules that may contribute to their combined therapeutic effects.

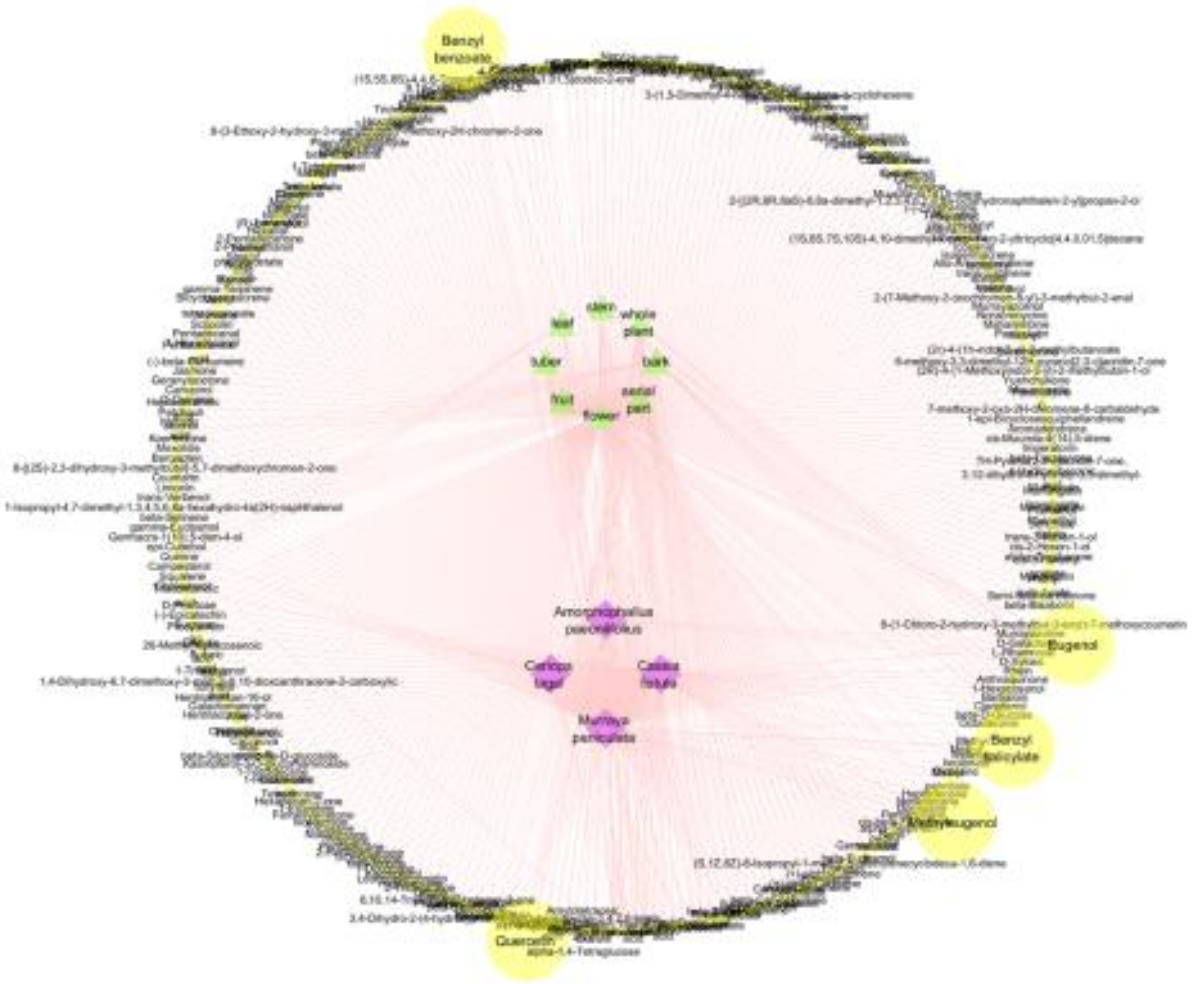

Figure 3 Network representation of key phytocompounds from *Cassia fistula, Ceriops tagal, Avicennia paconiifolius,* and *Mimosa panicula*, traditionally used in the treatment of visceral leishmaniasis.

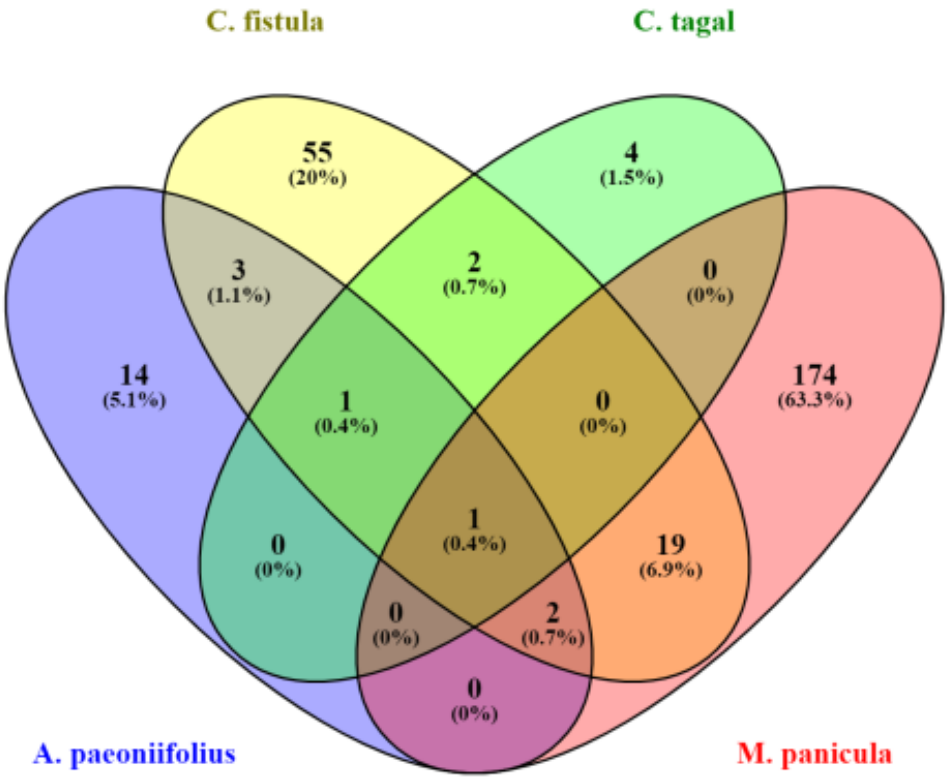

Figure 4 Venn diagram illustrating the overlap of phytochemical compounds among four medicinal plants: *Cassia fistula*, *Ceriops tagal*, *Avicennia paconiifolius*, and *Mimosa panicula*.

Table 1 Pharmacokinetic and Drug-Likeness Evaluation of Selected Phytochemicals.

Compounds	Number of Lipinski's rule of 5 violations	Lipinski's rule of 5	Number of Ghose rule violations	Ghose rule	Veber rule	Egan rule	GSK 4/400 rule	Pfizer 3/75 rule	drug-likeness score
Triacontane	1	Passed	3	Failed	Bad	Bad	Bad	Bad	0.12
Betulinic acid	1	Passed	3	Failed	Good	Bad	Bad	Bad	0.44
Oxalic acid	0	Passed	4	Failed	Good	Good	Good	Bad	0.38
Quercetin	0	Passed	0	Passed	Good	Good	Good	Good	0.43
Fucosterol	1	Passed	3	Failed	Good	Bad	Bad	Bad	0.42
Tannic acid	1	Passed	3	Failed	Good	Bad	Bad	Bad	0.42
Stigmasterol	1	Passed	2	Failed	Good	Bad	Bad	Bad	0.46
beta-Sitosterol	1	Passed	2	Failed	Good	Bad	Bad	Bad	0.44
beta-Bisabolene	1	Passed	0	Passed	Good	Good	Bad	Bad	0.56
Octadecane	1	Passed	1	Failed	Bad	Bad	Bad	Bad	0.27
Methyl salicylate	0	Passed	3	Failed	Good	Good	Good	Bad	0.61
Eugenol	0	Passed	0	Passed	Good	Good	Good	Bad	0.69
Methyl linoleate	1	Passed	1	Failed	Bad	Good	Bad	Bad	0.22
Methyl linolenate	1	Passed	1	Failed	Bad	Good	Bad	Bad	0.25
Methyleugenol	0	Passed	0	Passed	Good	Good	Good	Bad	0.66
Eicosane	1	Passed	1	Failed	Bad	Bad	Bad	Bad	0.24
Methyl palmitate	1	Passed	1	Failed	Bad	Good	Bad	Bad	0.3
Benzyl salicylate	0	Passed	0	Passed	Good	Good	Good	Bad	0.82
Heptadecane	1	Passed	1	Failed	Bad	Bad	Bad	Bad	0.29
Nonadecane	1	Passed	1	Failed	Bad	Bad	Bad	Bad	0.25
Docosane	1	Passed	1	Failed	Bad	Bad	Bad	Bad	0.21
Pentacosane	1	Passed	2	Failed	Bad	Bad	Bad	Bad	0.17
Asperglaucide	0	Passed	0	Passed	Bad	Good	Bad	Bad	0.47
cis-beta-Farnesene	1	Passed	0	Passed	Good	Good	Bad	Bad	0.39
alpha-Terpineol	0	Passed	1	Failed	Good	Good	Good	Bad	0.58
Nerol	0	Passed	1	Failed	Good	Good	Good	Bad	0.62
Phytol	1	Passed	1	Failed	Bad	Bad	Bad	Bad	0.39
Nerolidol	0	Passed	0	Passed	Good	Good	Bad	Bad	0.63
Ethyl butyrate	0	Passed	2	Failed	Good	Good	Good	Bad	0.52
Stearic acid	1	Passed	1	Failed	Bad	Bad	Bad	Bad	0.34
Oleic acid	1	Passed	1	Failed	Bad	Bad	Bad	Bad	0.29
Lupeol	1	Passed	3	Failed	Good	Bad	Bad	Bad	0.42
Palmitic acid	1	Passed	0	Passed	Bad	Good	Bad	Bad	0.41
D-Glucose	0	Passed	2	Failed	Good	Bad	Good	Good	0.29

3.2. Protein–protein interaction (PPI) network construction

To investigate the molecular mechanisms underlying the therapeutic potential of selected phytochemicals against visceral leishmaniasis, a protein–protein interaction (PPI) network is constructed based on shared targets between compounds and the disease. Initially, predicted target genes of the screened phytochemicals are retrieved via the SuperPred server and standardized using UniProt annotations. Disease-associated genes for visceral leishmaniasis are obtained from GeneCards. Intersection analysis identified 27 overlapping targets between the predicted phytochemical targets (Set A) and leishmaniasis-related genes (Set B), as shown in the Venn diagram (Figure 5). Set A contained 1 element (0.2%), Set B contained 561 elements (95.2%), and their intersection included 27 elements (4.6%). These 27 shared targets are submitted to the STRING database to construct a PPI network with medium confidence (score ≥ 0.4), limited to Homo sapiens. The resulting network comprised 27 nodes and 613 edges, with an average node degree of 23.1 and an average clustering coefficient of 0.723, indicating a highly interconnected and modular structure. The observed number of interactions far exceeded the expected 290 edges, supported by a strong PPI enrichment p-value (< 1.0e-16). The constructed PPI network is presented in Figure 6.

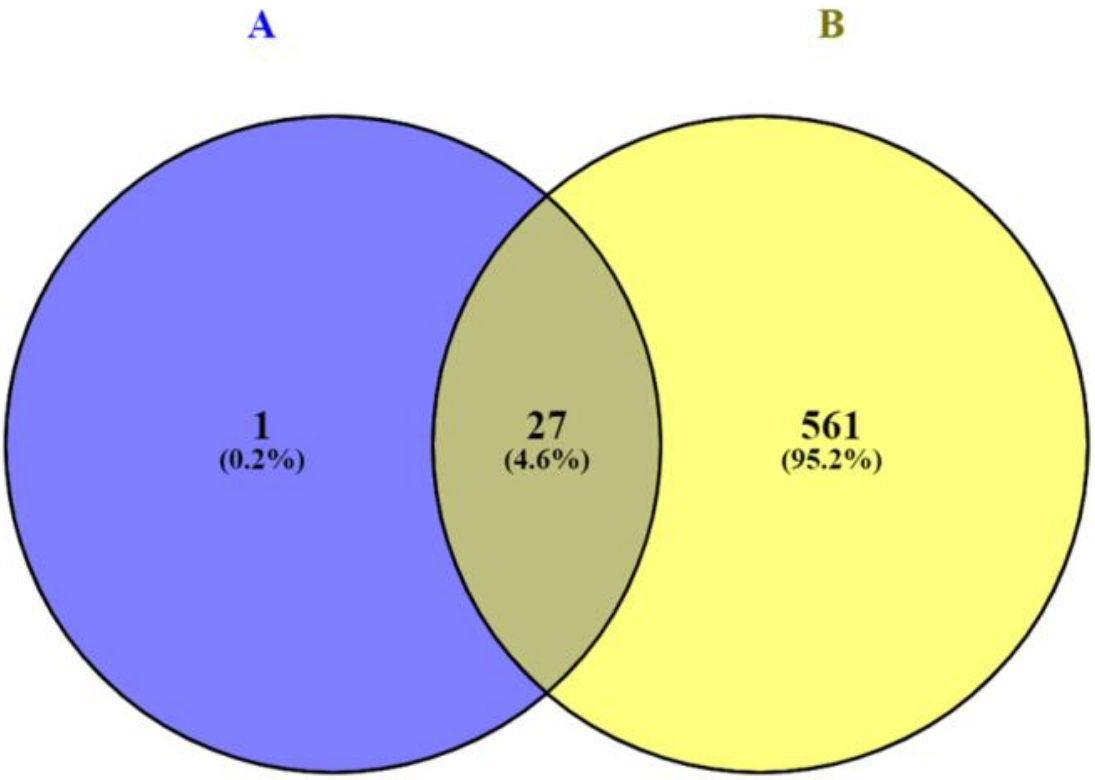

Figure 5 Venn diagram showing the overlap between predicted targets of screened phytochemicals (Set A) and visceral leishmaniasis-associated genes (Set B). Set A contains 1 element (0.2%), Set B contains 561 elements (95.2%), and their intersection includes 27 shared targets (4.6%) potentially relevant for therapeutic modulation.

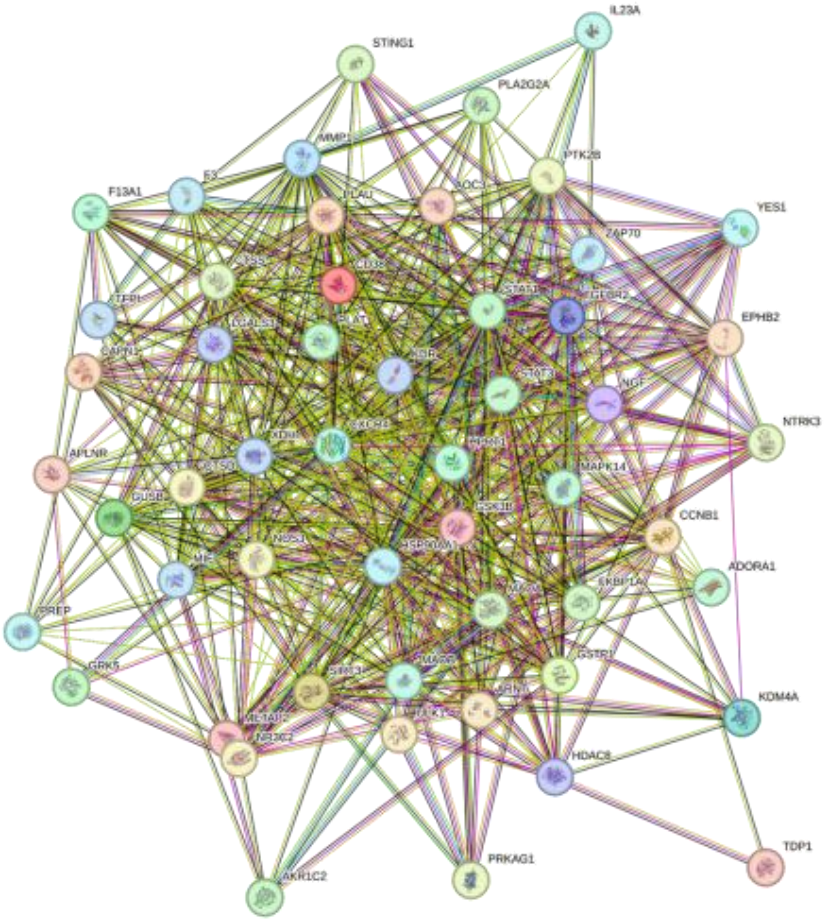

Figure 6 Protein–protein interaction (PPI) network of 27 shared targets between phytochemical-predicted proteins and visceral leishmaniasis-associated genes. Nodes represent proteins, and edges represent predicted functional associations with a confidence score ≥ 0.4. The network exhibits high connectivity and modularity, indicating potential coordinated involvement in disease-related pathways.

3.3. GO enrichment and KEGG pathway analysis

Gene Ontology (GO) enrichment and Kyoto Encyclopedia of Genes and Genomes (KEGG) pathway analyses are conducted to explore the biological roles and pathways linked to the phytochemical targets. Figure 7 presents three interconnected enrichment plots illustrating the most significant biological processes, molecular functions, and cellular components associated with the targets. The biological processes with the highest enrichment scores include cellular response to biotic stimulus, regulation of chemokine production, and response to oxidative stress, emphasizing immune and inflammatory responses. Molecular functions such as cytokine activity, nucleosidase activity, and transcription factor binding are notably enriched, highlighting the involvement of signaling and enzymatic regulatory mechanisms. Cellular components enriched include membrane-associated structures like the external side of the plasma membrane, secretory granules, and peroxisomal matrix, suggesting the spatial context of these biological activities. This coordinated enrichment across

processes, functions, and cellular locations underscores a complex and integrated cellular response to bacterial components and inflammatory signaling, reflecting the multifaceted mode of action of the phytochemicals. Figure 8 further illustrates a network diagram of these enriched pathways and bioactive compounds. Central nodes such as Eugenol and Methyleugenol connect to key pathways including Th17 cell differentiation and chemical carcinogenesis. The network highlights intricate interactions involving inflammatory mediators (TNF, IL-6, IL-1B), oxidative stress regulators (HMOX1), and cancer-related factors (ABCB1, ABCC1, STAT1), pointing to the therapeutic potential of these phytochemicals in modulating inflammation, immune response, and carcinogenic pathways. These enrichment analyses highlight key mechanisms through which the selected phytochemicals may exert antileishmanial effects. The involvement of Th17 cell differentiation genes suggests a role in modulating T-helper cell [16], while enrichment of TNF and IL-6 implies potential anti-inflammatory activity relevant to Leishmania infection [17]. Targets like HMOX1 point to antioxidant effects, supporting parasite clearance via oxidative stress modulation [18]. The presence of ABC transporters and STAT1, associated with carcinogenesis, indicates broader protective roles against inflammation-driven pathology [19]. Overall, phytochemicals such as Eugenol and Methyleugenol may act on multiple immune and redox pathways, offering therapeutic potential against visceral leishmaniasis [20].

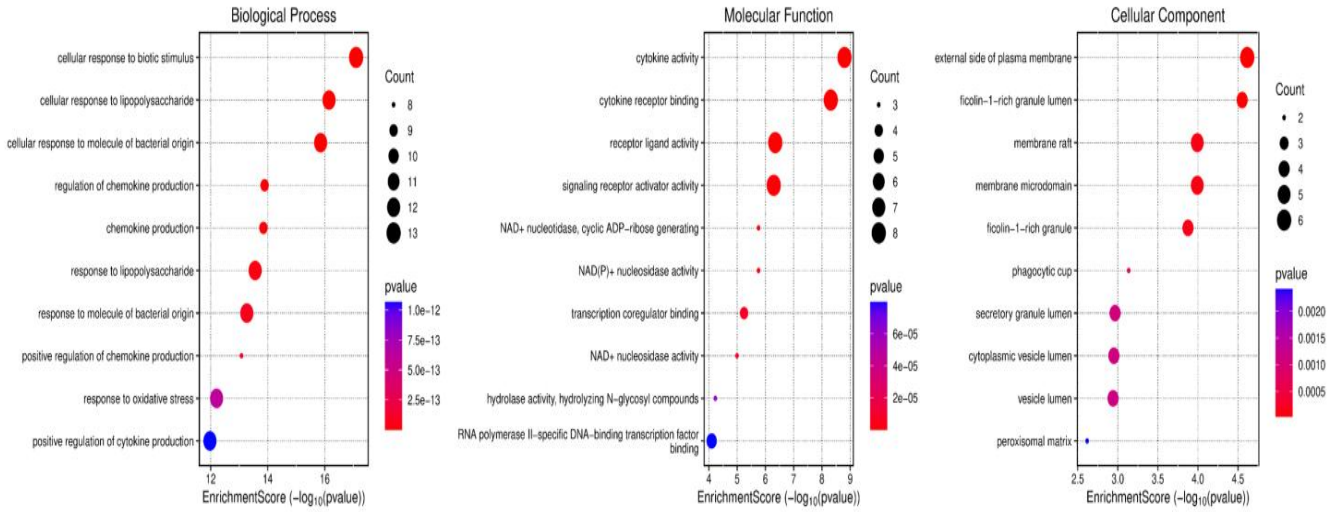

Figure 7 GO enrichment analysis visualized as three related plots representing the top enriched biological processes, molecular functions, and cellular components associated with phytochemical targets.

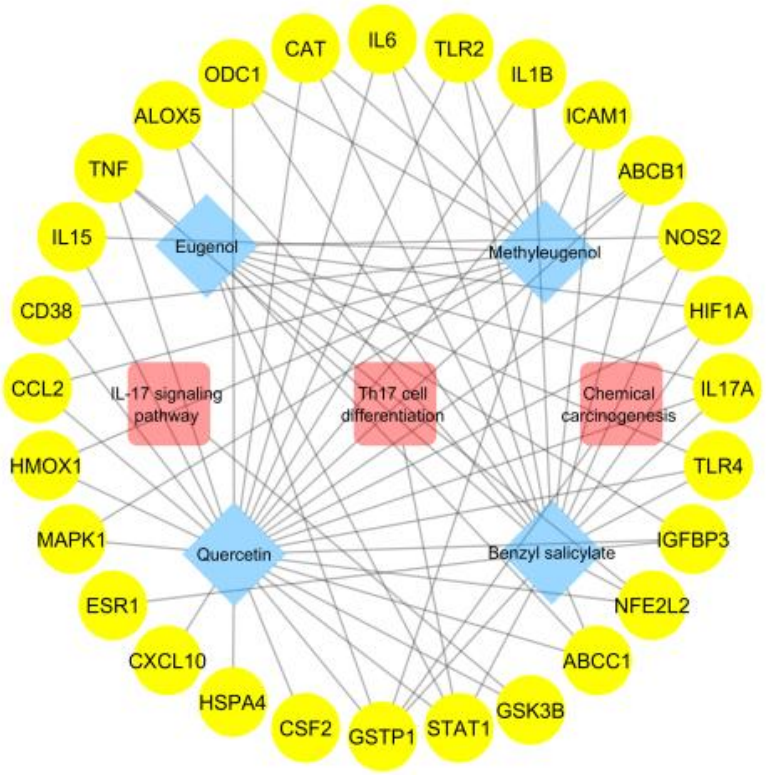

Figure 8 Network diagram integrating GO and KEGG pathway analysis, showing relationships between key phytochemicals (e.g., Eugenol, Methyleugenol) and biological pathways such as Th17 cell differentiation, inflammation, oxidative stress, and chemical carcinogenesis.

3.4. Molecular docking study

To validate the docking protocol, the co-crystallized ligand is re-docked into the active site of the target protein (PDB ID: 6TUU). As shown in Figure 9, the re-docked pose (yellow) aligned perfectly with the original crystallographic conformation (blue), yielding an RMSD of 0.000 Å based on 14 atoms [21-25]. This precise overlap confirms the reliability and accuracy of the docking procedure [26-28]. The binding affinities and molecular interactions of selected phytochemicals, Eugenol, Methyleugenol, Benzyl salicylate, and Quercetin are then compared to the reference ligand (Table 2). Quercetin exhibited the strongest predicted binding affinity (–7.2 kcal/mol), followed by the co-crystallized ligand (–7.0 kcal/mol), Benzyl salicylate (–6.7 kcal/mol), Eugenol (–6.0 kcal/mol), and Methyleugenol (–4.7 kcal/mol). Quercetin exhibited the most favorable binding affinity [29, 30]. This is consistent with previous in silico and in vitro studies reporting Quercetin's broad-spectrum antiprotozoal activity [20, 31-35]. However, the strength of binding must be interpreted alongside binding site similarity and interaction quality. Notably, Eugenol shares the same binding pocket as the co-crystallized ligand, as confirmed by the protein surface analysis in Figure 10. This compound forms hydrogen bonds with key active site residues: Lys144, Gly143, Ser142, Thr145 that are also engaged by the reference ligand. It further maintains hydrophobic contacts with Phe140 and Gly141, supporting a similar binding mode and potential functional mimicry [36-40]. These observations support the potential of Eugenol to act as a competitive inhibitor by mimicking the native ligand's interaction

profile. Similar findings have been reported for Eugenol's antileishmanial effects, where its ability to disrupt parasite membrane integrity and enzyme function has been highlighted [21, 22, 41-45]. In contrast, while Quercetin displayed the highest binding affinity, its interactions involved entirely different residues located outside the canonical binding site, suggesting a different binding mode [46-50]. Benzyl salicylate also interacted with a distinct region of the protein, engaging peripheral residues such as Asn283, Arg257, and His303, with no overlap with the key catalytic residues [51-55]. These observations suggest that Eugenol, despite having a slightly lower binding energy than Quercetin, is the most pharmacologically relevant ligand due to its ability to occupy the correct active site and replicate critical interactions of the co-crystallized ligand [56-60].

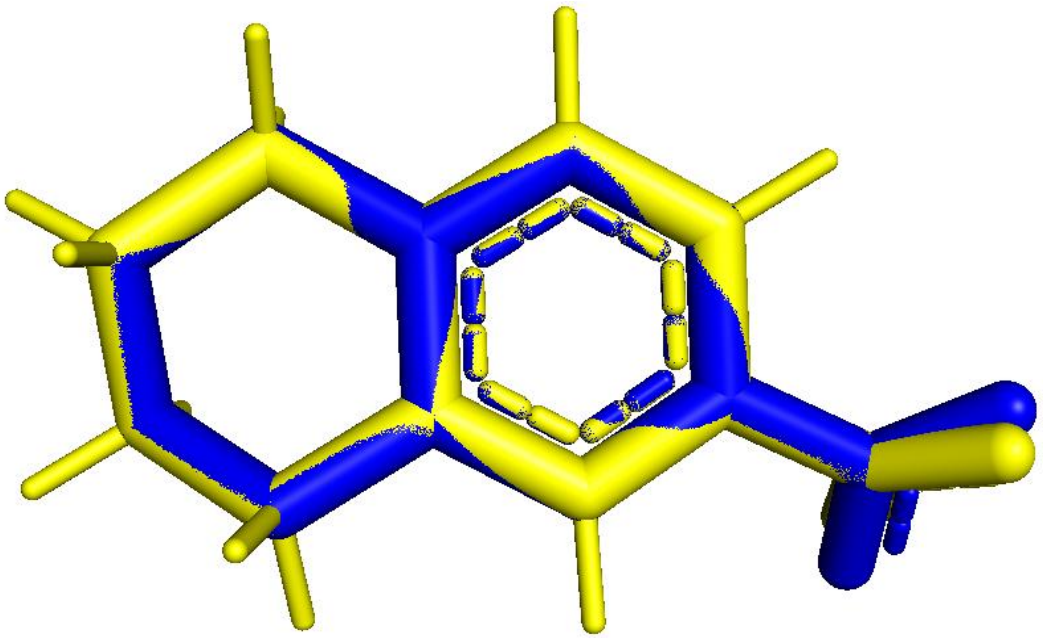

Figure 9 Conformational alignment of the re-docked pose (yellow) with the co-crystallized ligand (blue) in the active site. An RMSD of 0.000 Å (14 atoms) confirms precise overlap and docking accuracy.

Table 2 Binding affinity and molecular interactions of target protein with the selected ligands and the reference co-crystallized ligand.

Ligands	PubChem ID	Estimated free energy of binding (kcal/mol)	Hydrogen bonding	Hydrophobic contact
2-oxopentadecanoyl coenzyme A	Co-crystallized ligand	-7.0	Gly143 Ser142 Thr145 Lys144	Phe140 Gln146 Gly141
Benzyl salicylate	8363	-6.7	Asn283	Arg257 His303 Leu261 Gln258 Thr241 Arg245 Leu305 Glu135 Phe137 Val285
Eugenol	3314	-6.0	Lys144 Gly143	Ser142 Phe140 Gly141 Gln284 Thr145 Thr176
Methyleugenol	7127	-4.7	Arg312	Phe137 Leu305 Glu135 Ile304 Val285
Quercetin	5280343	-7.2	Gln131 Leu124 Arg112 Ser308	Gly125 Glu129 Leu311 Leu333 Thr310 Ala132 His269 Ala309

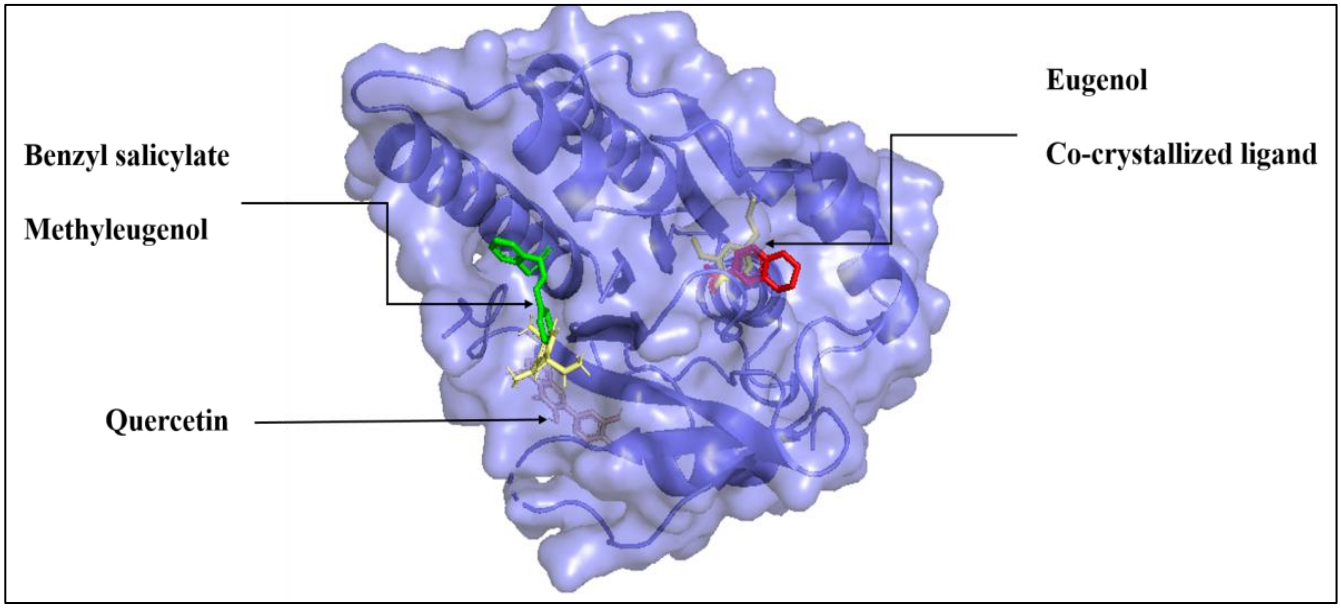

Figure 10 Protein surface representation highlighting various ligand-binding cavities. The main binding cavity contains both the co-crystallized ligand and Eugenol, indicating that Eugenol occupies the same active site as the reference compound.

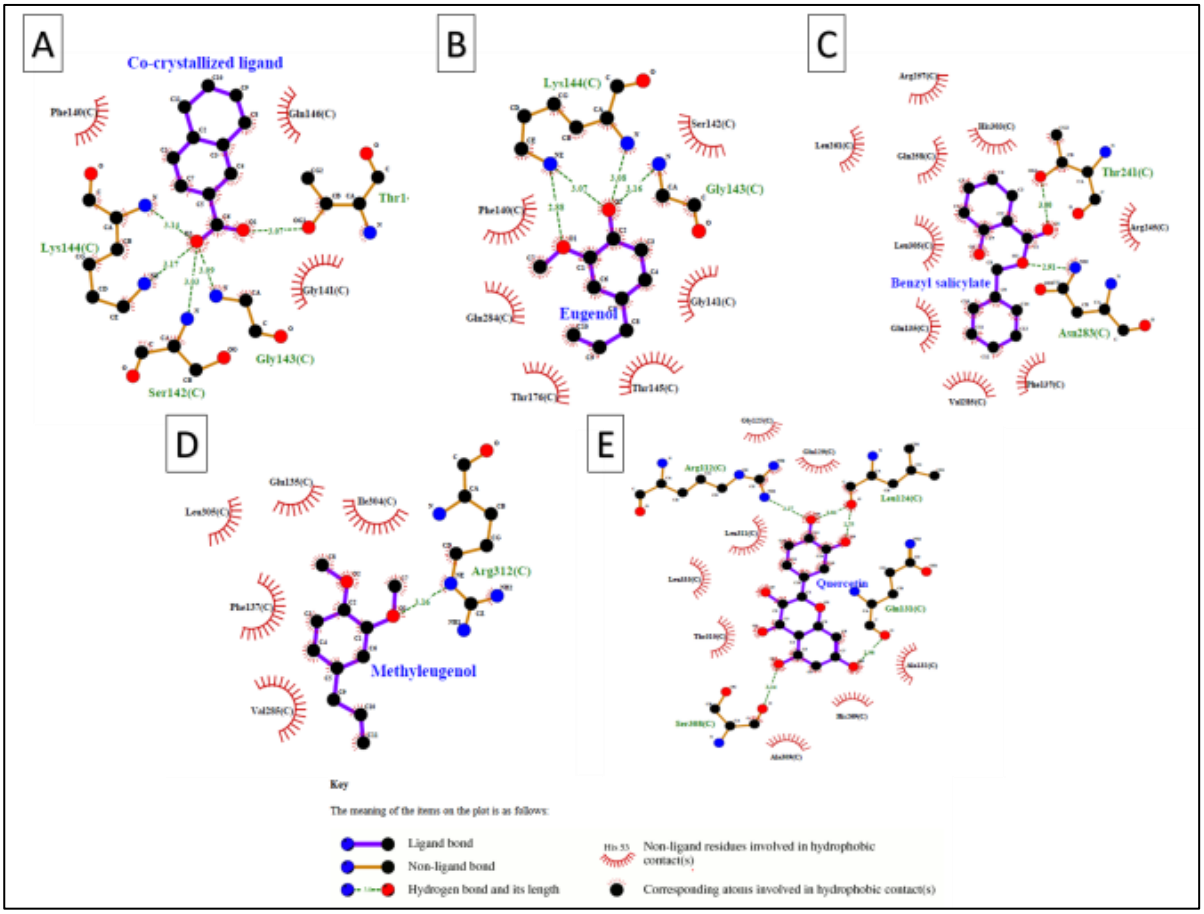

Figure 11 LigPlot+ interaction diagrams showing the binding modes of (A) the co-crystallized ligand, (B) Eugenol, (C) Benzyl salicylate, (D) Methyleugenol, and (E) Quercetin within the active site of 6TUU. Hydrogen bonds are depicted as green dashed lines, and hydrophobic interactions are shown as red spoked arcs, illustrating the key contacts stabilizing each ligand–protein complex.

3.5. Effect of nanotechnology on drug discovery and molecular interaction analysis

The integration of nanotechnology concepts provides deeper insight into the molecular interactions between phytochemicals and target proteins. Nanoscale analysis enhances the understanding of binding mechanisms, stability, and interaction dynamics. Nanotechnology also supports the development of nano-drug delivery systems that can improve the bioavailability and therapeutic efficacy of compounds such as Eugenol [61-65]. These advancements highlight the importance of nanotechnology in accelerating drug discovery for parasitic diseases [66-70]. Table 3 presents a comparative evaluation of conventional and nanotechnology-enhanced drug discovery approaches, demonstrating improved interaction accuracy, bioavailability, and therapeutic efficiency [71-74].

Table 3 Comparison between conventional and nanotechnology-enhanced approaches in molecular docking and drug discovery for visceral leishmaniasis.

Parameter	Conventional Approach	Nano-Enhanced Approach
Binding Analysis	Standard docking	Nanoscale precision
Drug Delivery	Limited	Targeted nano-delivery
Bioavailability	Moderate	Enhanced
Interaction Accuracy	Good	High
Therapeutic Efficiency	Moderate	Improved

Figure 12 presents the impact of nanotechnology on drug discovery, highlighting enhanced molecular interaction precision and improved therapeutic efficiency.

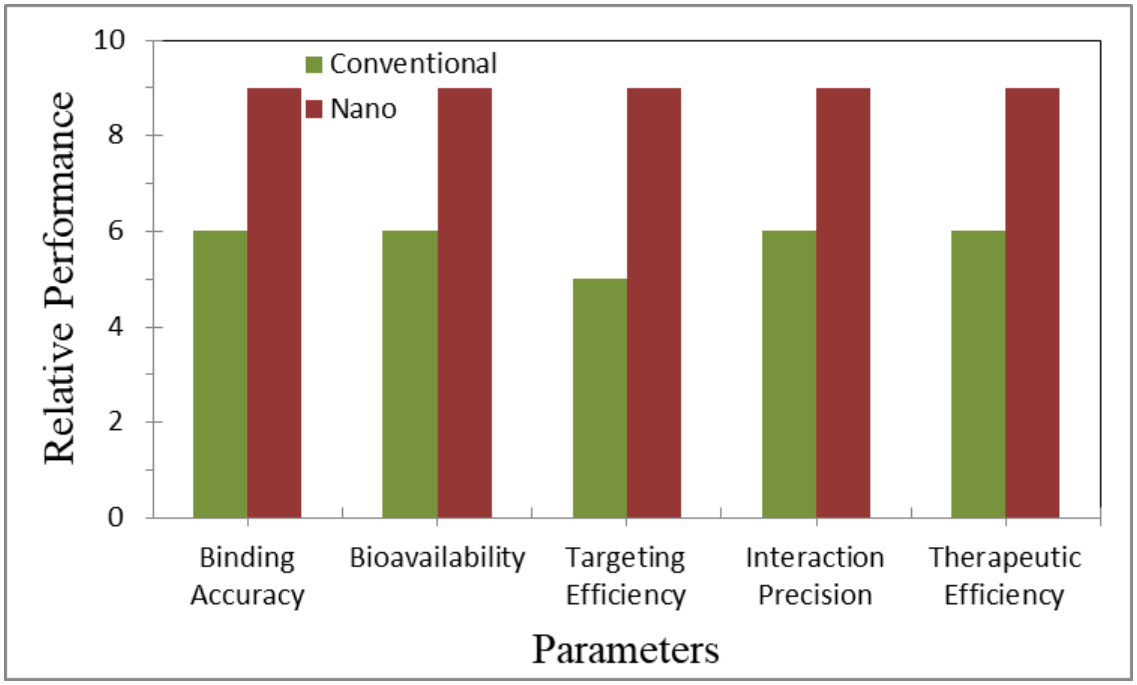

Figure 12 Effect of nanotechnology on molecular docking and drug delivery efficiency of phytochemicals targeting visceral leishmaniasis.

4. CONCLUSIONS

This study demonstrated the power of integrating network pharmacology and molecular docking to identify promising lead compounds from traditional medicinal plants. Among the screened phytochemicals, Eugenol stood out as a key candidate with significant overlap in binding mode with the co-crystallized ligand in the 6TUU protein, which is functionally relevant in visceral leishmaniasis. The compound's favorable pharmacokinetic properties, binding site fidelity, and biological pathway enrichment suggest its potential for further preclinical validation. These findings support the continued exploration of phytochemicals as rich sources for anti-leishmanial drug discovery. The integration of nanotechnology into network pharmacology and molecular docking provides a powerful framework

for improving drug discovery against visceral leishmaniasis. Nanotechnology enhances molecular interaction analysis, improves bioavailability, and supports targeted drug delivery, making it a promising approach for developing effective antileishmanial therapies.

References

[1] Haitham Mohammed Ibrahim Al-Zuhairi, Iqbal alshalal, Hind H. Abbood, M. Al Nuaimi, Experimental and Theoretical NANOTECHNOLOGY, 10 (2026) 855 https://doi.org/10.56053/10.S.855
[2] C. H. Costa, et al., Pathogens, 12 (2023) 969. https://doi.org/10.3390/pathogens12070969
[3] C. Cosma, et al., Tropical Medicine and Infectious Disease, 9 (2024) 258. https://doi.org/10.3390/tropicalmed9110258
[4] A. Ponte-Sucre, et al., PLoS Neglected Tropical Diseases, 11 (2017) e0006052. https://doi.org/10.1371/journal.pntd.0006052
[5] S. L. Croft, S. Sundar, A. H. Fairlamb, Clinical Microbiology Reviews, 19 (2006) 111. https://doi.org/10.1128/CMR.19.1.111-126.2006
[6] B. Chopra, A. K. Dhingra, Phytotherapy Research, 35 (2021) 4660. https://doi.org/10.1002/ptr.7094
[7] M. Wink, Molecules, 17 (2012) 12771. https://doi.org/10.3390/molecules171112771
[8] Raghad A. Rasheed, Maysoon F. A. Alias, Experimental and Theoretical NANOTECHNOLOGY, 10 (2026) 1139 https://doi.org/10.56053/10.S.1139
[9] A. L. Hopkins, Nature Chemical Biology, 4 (2008) 682. https://doi.org/10.1038/nchembio.118
[10] L. Pinzi, G. Rastelli, International Journal of Molecular Sciences, 20 (2019) 4331. https://doi.org/10.3390/ijms20184331
[11] X.-Y. Meng, et al., Current Computer-Aided Drug Design, 7 (2011) 146. https://doi.org/10.2174/157340911795677602
[12] F. Boudou, et al., Frontiers in Chemistry, 12 (2024) 1508603. https://doi.org/10.3389/fchem.2024.1508603
[13] F. Boudou, et al., Frontiers in Chemistry, 13 (2025) 1509913. https://doi.org/10.3389/fchem.2025.1509913
[14] S. C. Gonçalves-de-Albuquerque, et al., Frontiers in Immunology, 8 (2017) 1437. https://doi.org/10.3389/fimmu.2017.01437
[15] W. N. Oliveira, et al., Cytokine, 66 (2014) 127. https://doi.org/10.1016/j.cyto.2013.12.001
[16] K. Becker, S. Koncarevic, N. H. Hunt, Molecular Approaches to Malaria (2005) 365. https://doi.org/10.1007/0-387-29085-2_18
[17] G. Kapoor, et al., Cancer Investigation, 43 (2025) 1. https://doi.org/10.1080/07357907.2024.2430607
[18] H. Memariani, M. Memariani, A. Ghasemian, BioMed Research International, 2024 (2024). 7632408. https://doi.org/10.1155/2024/7632408
[19] T. Ueda-Nakamura, et al., Parasitology International, 55 (2006) 99. https://doi.org/10.1016/j.parint.2005.11.046
[20] M. A. Ungogo, et al., Frontiers in Chemistry, 8 (2020) 617448. https://doi.org/10.3389/fchem.2020.617448
[21] I. Alshalal, H. M. I. Al-Zuhairi, A. A. Abtan, M. Rasheed, M. K. Asmail. J. Mech. Behav. Mater. 32 (2023) 1. https://doi.org/10.1515/jmbm-2022-0280
[22] M. Sellam, M. Rasheed, S. Azizi, T. Saidani. Ceram. Int. 50 (2024) 20917. https://doi.org/10.1016/j.ceramint.2024.03.094

[23] O. Alabdali, S. Shihab, M. Rasheed, T. Rashid. 3rd inter. Scient. conf. alkafeel univ. (ISCKU 2021) 2386 (2022) 050019. https://doi.org/10.1063/5.0066860
[24] M. Rasheed, O. Alabdali, S. Shihab, A. Rashid, T. Rashid, J. Phys.: Conf. Ser. 1999 (2021) 012078. https://doi.org/10.1088/1742-6596/1999/1/012078
[25] N. Assoudi et al. Opt. Quant. Electron. 54 (2022) 9. https://doi.org/10.1007/s11082-022-03927-x
[26] R. Jalal, S. Shihab, M.A. Alhadi, M. Rasheed, J. Phys.: Conf. Ser. 1660 (2020) 012090. https://doi.org/10.1088/1742-6596/1660/1/012090
[27] S. Shihab, M. Rasheed, O. Alabdali, A.A. Abdulrahman, J. Phys.: Conf. Ser. 1879 (2021) 022120. https://doi.org/10.1088/1742-6596/1879/2/022120
[28] A. Keziz, M. Heraiz, M. RASHEED, A. Oueslati. Mater Chem. Phys. 325 (2024) 129757. https://doi.org/10.1016/j.matchemphys.2024.129757
[29] D. Kherifi, A. Keziz, M. Rasheed, A. Oueslati. Ceram. Int. 50 part A (2024) 30175. https://doi.org/10.1016/j.ceramint.2024.05.317
[30] A. Jaber, M. Ismael, T. Rashid, M. A. Sarhan, M. Rasheed, I. M. Sala. Eureka: Phys. Eng. 4 (2023) 29. https://doi.org/10.21303/2461-4262.2023.002770
[31] T. Rashid, M. M. Mokji, M. Rasheed. J. Optics 54 (2024) 3490. https://doi.org/10.1007/s12596-024-02080-w
[32] H. K. Aity, E. Dhahri, M. Rasheed. Ceram. Int. 50 (2024) part B 54666. https://doi.org/10.1016/j.ceramint.2024.10.324
[33] M. Rasheed, S. Shihab, O. Alabdali, A. Rashid, T. Rashid, J. Phys.: Conf. Ser. 1999 (2021) 012077. https://doi.org/10.1088/1742-6596/1999/1/012077
[34] M. Rasheed, M. Nuhad Al-Darraji, S. Shihab, A. Rashid, T. Rashid. J. Phys.: Conf. Ser. 1963 (2021) 012058. https://doi.org/10.1088/1742-6596/1963/1/012058
[35] A. Keziz, M. Heraiz, F. Sahnoune, M. Rasheed, Ceram. Int. 49 (2023) 32989. https://doi.org/10.1016/j.ceramint.2023.07.275
[36] E. Kadri, K. Dhahri, R. Barillé, M. Rasheed. Phase Transi. 94 (2021) 65. https://doi.org/10.1080/01411594.2020.1832224
[37] D. Bouras, M. Rasheed, Opt. Quantum Electron. 54 (2022) 12. https://doi.org/10.1007/s11082-022-04161-1
[38] A. Zubaidi, L.M. Asaad, I. Alshalal, M. Rasheed, J. Mech. Behav. Mater. 32 (2023) 1. https://doi.org/10.1515/jmbm-2022-0302
[39] M. Rasheed et al., J. Phys.: Conf. Ser. 1999 (2021) 012080. https://doi.org/10.1088/1742-6596/1999/1/012080
[40] M. Rasheed, M.N. Al-Darraji, S. Shihab, A. Rashid, T. Rashid, J. Phys.: Conf. Ser. 1963 (2021) 012059. https://doi.org/10.1088/1742-6596/1963/1/012059
[41] M. Enneffatia, M. Rasheed, B. Louati, K. Guidara, S. Shihab, R. Barillé, J. Phys.: Conf. Ser. 1795 (2021) 012050. https://doi.org/10.1088/1742-6596/1795/1/012050
[42] M. Rasheed, O.Y. Mohammed, S. Shihab, A. Al-Adili, J. Phys.: Conf. Ser. 1795 (2021) 012043. https://doi.org/10.1088/1742-6596/1795/1/012043
[43] A.H. Ali, A.S. Jaber, M.T. Yaseen, M. Rasheed, O. Bazighifan, T.A. Nofal, Complexity 2022 (2022) 1. https://doi.org/10.1155/2022/9367638
[44] M. Rasheed, et al., J. Adv. Biotechnol. Exp. Ther. 6 (2023) 495. https://doi.org/10.5455/jabet.2023.d144
[45] M. Rasheed, I. Alshalal, A.A. Ashed, M.A. Sarhan, A.S. Jaber, Indones. J. Electr. Eng. Comput. Sci. 33 (2024) 653. https://doi.org/10.11591/ijeecs.v33.i1.pp653-660
[46] I.M. Mohammed, M. Rasheed, AIP Conf. Proc. 3321 (2025) 020026. https://doi.org/10.1063/5.0289719

[47] F. Boudou, A. Belakredar, A. Berkane, M. Rasheed. Not. Sci. Biol. 17 (2025) 12183. https://doi.org/10.55779/nsb17212183
[48] F. Boudou, et al., Not. Sci. Biol. 17 (2025) 12593. https://doi.org/10.55779/nsb17312593
[49] F. Boudou, A. Guendouzi, A. Belkredar. M. Rasheed, Not. Sci. Biol. 16 (2024) 13837. https://doi.org/10.55779/nsb16211837
[50] R.S. Mahmood et al. J. Mech. Behav. Mater. 34 (2025) 1. https://doi.org/10.1515/jmbm-2025-0040
[51] T. Rashid, M.M. Mokji, M. Rasheed, J. Mech. Behav. Mater. 34 (2025) 77. https://doi.org/10.1515/jmbm-2025-0074
[52] M. Rasheed, M. N. Mohammedali, F. A. Sadiq, M. A. Sarhan, T. Saidani. J. Optics (New Delhi. Print) 54 (2024) 3490. https://doi.org/10.1007/s12596-024-01928-5
[53] A.J. Hussein, M.N. Al-Darraji, M. Rasheed, M.A. Sarhan, IOP Conf. Ser.: Earth Environ. Sci. 1262 (2023) 022007. https://doi.org/ 10.1088/1755-1315/1262/2/022007
[54] A.J. Hussein, M.N. Al-Darraji, M. Rasheed, M.A. Sarhan, IOP Conf. Ser.: Earth Environ. Sci. 1262 (2023) 022005. https://doi.org/10.1088/1755-1315/1262/2/022005
[55] T. Saidani, M. Rasheed, I. Alshalal, A.A. Rashed, M.A. Sarhan, R. Barillé, Res. Eng. Struct. Mater. 10 (2024) 743. http://dx.doi.org/10.17515/resm2023.21ma0922rs
[56] M. A. Sarhan, S. Shihab, B. E. Kashem, M. Rasheed, J. Phy.: Conf. Ser., 1879 (2021) 022122. https://doi.org/10.1088/1742-6596/1879/2/022122
[57] M. Rasheed, O. Alabdali, S. Shihab, J. Phy.: Conf. Ser. 1879 (2021) 032120. https://doi.org/10.1088/1742-6596/1879/3/032120
[58] M. Rasheed, R. Barillé, J. Non-Cryst. Solids., 476 (2017) 1. https://doi.org/10.1016/j.jnoncrysol.2017.04.027
[59] M. Rasheed, R. Barillé, Opt. Quantum Electron. 49 (2017). https://doi.org/10.1007/s11082-017-1030-7
[60] F. Dkhilalli, S. M. Borchani, M. Rasheed, R. Barille, K. Guidara, M. Megdiche, J. Mater. Sci. Mater. Electron, 29 (2018) 6297. https://doi.org/10.1007/s10854-018-8609-z
[61] A. Boumezoued, K. Guergouri, Régis Barillé, Rechem Djamil, Mourad Zaabat, M. Rasheed, J. Alloys Compd. 791 (2019) 550. https://doi.org/10.1016/j.jallcom.2019.03.251
[62] N. Ben Azaza et al., Opt. Mater., 96 (2019) 109328. https://doi.org/10.1016/j.optmat.2019.109328
[63] Areej Adnan Hateef, Essebti Dhahri, M. Rasheed, Habiba Kadhim, Z. Abbas, N. Hassan, Physics and Chemistry of Solid State, 25 (2024) 801. https://doi.org/10.15330/pcss.25.4.801-810
[64] M. Rasheed, SuhaShihab, O. Alabdali, H. H. Hassan, J. Phys. Conf. Ser., 1879 (2021) 032113. https://doi.org/10.1088/1742-6596/1879/3/032113
[65] H. K. Aity, M. Rasheed, E. Dhahri, A. A. Hateef, T. Saidani, Journal of Materials Science, 61 (2026) 6226. https://doi.org/10.1007/s10853-026-12241-w
[66] T. Saidani, S. Mokhtari, M. Rasheed, H. Lahmar, M. Trari, Journal of the Indian Chemical Society, 103 (2026) 102499. https://doi.org/10.1016/j.jics.2026.102499
[67] M. RASHEED, A. Khaleefah, Materials Chemistry and Physics, 353 (2026) 132112. https://doi.org/10.1016/j.matchemphys.2026.132112
[68] S. S. Batros, M. Rasheed, H. K. Aity, A. A. Hatef, T. Saidani, Materials Chemistry and Physics, 355 (2026) 132243. https://doi.org/10.1016/j.matchemphys.2026.132243
[69] A. Raghdi, M. Heraiz, M. Rasheed, A. Keziz, Journal of the Indian Chemical Society, 101 (2024) 101413. https://doi.org/10.1016/j.jics.2024.101413
[70] A. I. A. Ali, M. RASHEED, Experimental and Theoretical NANOTECHNOLOGY, 10 (2026) 277. https://doi.org/10.56053/10.s.277

[71] A. Khaleefah, M. RASHEED, Experimental and Theoretical NANOTECHNOLOGY, 10 (2026) 289. https://doi.org/10.56053/10.s.289
[72] Z. S. Ahmed, M. RASHEED, H. S. Ahmed, Experimental and Theoretical NANOTECHNOLOGY, 10 (2026) 329. https://doi.org/10.56053/10.s.329
[73] Z. S. Ahmed, M. RASHEED, H. S. Ahmed, Experimental and Theoretical NANOTECHNOLOGY, 10 (2026) 343. https://doi.org/10.56053/10.s.343
[74] A. I. A. Ali, M. RASHEED, Experimental and Theoretical NANOTECHNOLOGY, 10 (2026) 239. https://doi.org/10.56053/10.s.239

© 2026 The Authors. Published by LPCMA (https://etnano.com). This article is an open access article distributed under the terms and conditions of the Creative Commons Attribution license (http://creativecommons.org/licenses/by/4.0/).